Journal of the European Ceramic Society 16 (1996) 653–664

0955-2219/96/$15.00
0955-2219(95)00178-6

Microstructural Instability and the Resultant Strength of Si–C–O (Nicalon) and Si–N–C–O (HPZ) Fibres

R. Bodet,[a]* N. Jia[b] & R. E. Tressler[c]

[a]Laboratoire des Composites Thermostructuraux (UMR-47 CNRS-SEP-UB1), Domaine Universitaire, 3 allée de la Boétie, 33600 Pessac, France
[b]Analytical Sciences Laboratory, Allied Signal Inc., Morristown, NJ 07962-1021, USA
[c]Department of Materials Science and Engineering, The Pennsylvania State University, University Park, PA 16802, USA

(Received 25 March 1994; revised version received 12 September 1995; accepted 29 September 1995)

Abstract

Microstructural changes and the related strength degradation were investigated for Si–C–O Nicalon and Si–N–C–O HPZ fibres during heat treatments in air and argon at 1000–1400°C for 0·5 to 90 h. While the as-received Nicalon fibre contains β-SiC and carbon nanocrystals in an amorphous $SiO_{1\cdot12}C_{0\cdot44}$ phase, the HPZ fibre is completely amorphous. It is also inhomogeneous in surface composition compared with that of the bulk. The time-dependent strength degradation of the Nicalon fibre in argon is related to the gradual decomposition of the $SiO_{1\cdot12}C_{0\cdot44}$ phase from the surface which produces surface defects, β-SiC grain growth and intergranular porosity. The strength degradation of the HPZ fibre results from surface crystallization into α-SiO_2, Si_2N_2O and β-SiC. On the other hand, the HPZ fibre core — which has composition close to $SiN_{1\cdot02}C_{0.23}$ — shows structural stability for all heat treatment conditions.

1 Introduction

Advances in ceramic fibres are important in improving the performance of composite materials for high-temperature aerospace applications. The silicon carbide Nicalon® fibre, produced from the pyrolysis of polycarbosilane (PCS) according to Yajima's route,[1] is known to be chemically unstable at elevated temperature. Chemical reactions with the environment and thermal decomposition of the fibre lead to the formation of new populations of flaws, and result in chemical or physical modification of the fibre microstructure.[2–9] Moreover, transport processes such as viscous flow, which occurs during creep of the fibre, are highly temperature-dependent.[10] All these processes result in strength degradation in service. Recently, improvements in retained room-temperature strength and structure stability of Nicalon were observed after annealing for long periods of time in an environment containing carbon monoxide.[11] This treatment was successfully used to characterize the fibre creep behaviour with a rheological model for the viscous flow of a concentrated suspension.[12,13]

Several new ceramic fibres are currently under development. One fibre claimed to be compositionally and structurally stable to nearly 1400°C is the HPZ fibre, which is processed by pyrolysis of hydridopolysilazane.[9] Its structure can be described as a disordered $Si(N,C)_4$-based tetrahedral network containing only graphitic nanocrystals.[14] Unlike Nicalon fibre, studies on the thermal stability of HPZ fibre are still very limited. After thermal ageing in nitrogen or argon at 1200–1400°C, the fibre fracture strength was found to degrade significantly long before chemical and structural changes were evident.[3,15] Similar observations were reported after ageing in air for 2 h and in vacuum for 64 h at 1200°C, although the Young's modulus of the fibre remained unchanged after heat treatment.[16] A mechanism of property degradation involving diffusion-controlled reactions at flaw sites was postulated to explain this behaviour.[3] It was reported that the HPZ fibre aged in argon exhibits surface oxidation but much less change in the bulk compared with Nicalon.[3] Among several fibre-cordierite systems with a BN interphase, only those reinforced by the HPZ fibres experienced a strength loss (~60%) compared with the unreinforced matrix.[17] The brittle composite behaviour

*Now with Institute of Advanced Materials, Joint Research Center, Petten, The Netherlands.

was attributed to fibre degradation during the BN coating process at 600°C. Strong fibre–matrix bonding and strength degradation were also reported in the case of a chemical vapour deposition (CVD)-SiC coating (0·8 μm thick) on HPZ fibres.[16] Unlike Nicalon–glass matrix composites which develop a carbon interphase *in situ* during fabrication, those with HPZ fibres formed SiO_2-rich interfaces.[18–20] On the other hand, a deliberately formed CVD carbon coating on HPZ fibres prevented the occurrence of fibre–matrix interaction and properties approaching those of the best carbon-coated Nicalon composites were demonstrated.[18,19] The reasons for the high reactivity of the HPZ fibre with oxides, SiC and BN, and conversely its good compatibility with carbon, are not clear at this point.

Because the fibre–matrix interface is critical in many composite applications, chemical and structural characterizations of the HPZ fibre surface must be carried out. The main objective of this investigation was to compare the thermomechanical behaviours of PCS- and PCSZ-derived ceramic fibres in air and argon. The effects of long-term exposure on the microstructure and strength of these fibres were particularly studied by means of transmission electron microscope (TEM) analyses and room temperature tensile testing.

2 Experimental Procedure

Ceramic fibres investigated in this study were a commercial Nicalon fibre NLP 201 (Nippon Carbon, Yokohama, Japan) and an experimental HPZ fibre (Dow Corning, Midland, USA). The elemental compositions of the fibres obtained by EPMA are reported in Table 1. Both fibres are also known to contain some traces of hydrogen (~0·1 wt%).[14] The as-received fibres were washed in ultrasonically agitated baths of acetone, ethyl alcohol and distilled water, successively, except those exposed to heat treatments for which the organic sizing was burned off during the temperature rise.

A custom-built furnace consisting of a vertical alumina tube and six SiC heating elements was used for air and argon ageing at times from 0·5 to 90 h and temperatures between 1000 and 1400°C. Bundles of fibres were suspended by sewing them through either a carbon cloth (for argon heat treatments) or a silica cloth (for air heat treatments), which was placed inside the top part of the chamber. For argon heat treatments, a preliminary step consisting of evacuating the furnace for at least 1 h was used at the beginning of the heat treatment ($T < 550$°C) followed by a dwell time of 2 h at 550°C during which UHP argon gas (oxygen $<10^{-9}$ ppm) was introduced. An in-line oxygen sensor (zirconia cell) was used to determine the oxygen level.

Fibres were ground into powder in acetone and analysed by X-ray diffraction (XRD) (Rigaku Denki diffractometer) using Cu K_α radiation. Thermogravimetric analyses (TGA) were run on fibre bundles in dry argon with a heating rate of 100°C min^{-1}. The elemental composition of the as-received fibres was determined by electron probe microanalysis (EPMA) with a Camebax probe (model 75). X-ray photoelectron (XPS) and Auger electron (AES) spectroscopies were performed using an Al-targeted X-ray source in an ESCA/SAM/MACS system (Perkin–Elmer, model 560). The XPS data were calibrated using the Si 2p (101·1 eV) and C 1s (283·3 eV) binding energies for SiC. Samples were sputter-cleaned by 3 keV argon ion beams prior to analysis. The compositions were determined from the peak area for each element corrected for the relative sensitivity factor of XPS to the particular line. Individual filament fracture surfaces after strength tests were examined in an ISI-SX-40A scanning electron microscope (SEM). The fibre structure was analysed with a TEM microscope (Philips 420 T), using the bright field (BF), dark field (DF) and selected area electron diffraction (SAED) modes. TEM specimens were prepared either by gluing the fibres onto copper grids, followed by conventional ion-milling with argon ions (Gatan Dual Ion Mill), or by embedding the fibres in a very hard epoxy resin

Table 1. Elemental and molecular compositions of as-received Nicalon and HPZ fibres

	Elemental composition				*Molecular composition*			
Nicalon								
	Si	C	O			SiC	SiO_xC_y	C
at%	39	47	14		mol%	49	23	28
wt%	58	30	12		wt%	56	34	10
						$x = 1{\cdot}12$, $y = 0{\cdot}44$		
HPZ								
	Si	N	C	O		SiO_2	SiN_xC_y	C
at%	41	39	16	4	mol%	4	81	15
wt%	58	29	10	3	wt%	6	90	4
						$x = 1{\cdot}02$, $y = 0{\cdot}23$		

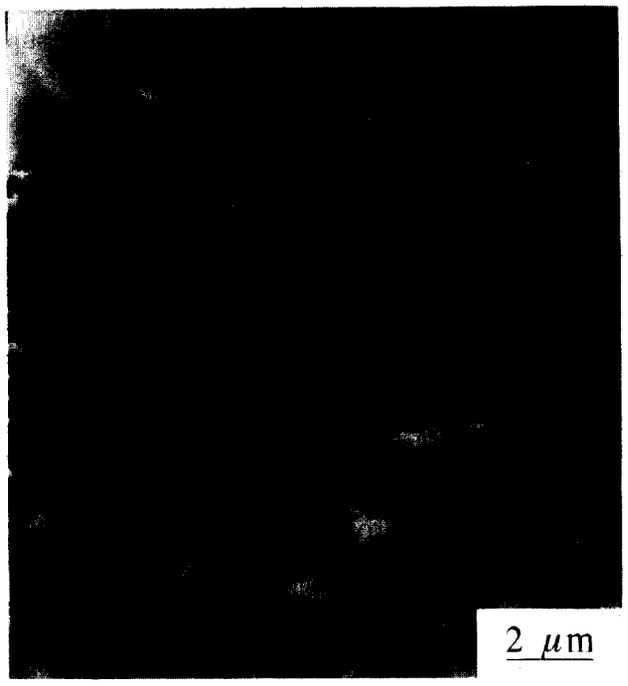

Fig. 1. Microtomed section of a Nicalon fibre after heat treatment in argon for 90 h at 1300°C, showing extensive surface degradation and grain growth.

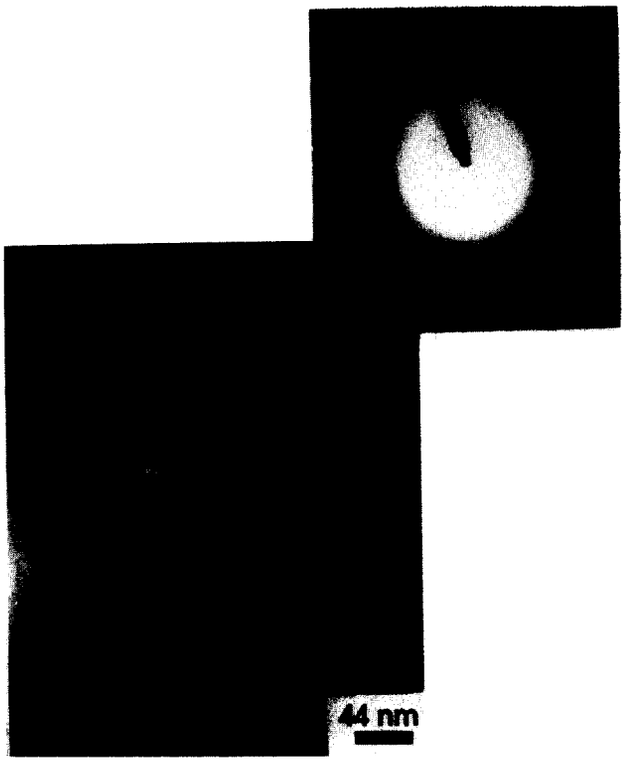

Fig. 2. TEM BF analysis of an as-received HPZ fibre. A typical globular pore found in the fibre core is shown by the arrow. The SAED pattern in the inset accounts for the amorphous character of the fibre bulk.

and subsequent microtoming of the resulting blocks with a diamond knife (Du Pont de Nemours). Although desired thicknesses could be obtained by microtomy, the fibre sections usually broke into small fragments oriented perpendicular to the knife travel. Minimum damage occurred for the most severely degraded fibres after long heat treatments, as shown in Fig. 1.

The short-term strength tests were performed on individual fibres in air at room temperature, all at the same crosshead speed of 0·5 mm min.$^{-1}$ The loading apparatus consisted of a table-top Instron tester (model 1102). The true elongation of the fibre was obtained by correcting the recorded elongation by taking into account a system compliance which is a function of both load-cell and grip deformations and fibre diameter.[21]

3 Results

3.1 Microstructure of as-received fibres

An average β-SiC grain size of 2·7 nm was obtained from an (1 1 1)-SiC dark-field image of the as-received Nicalon fibre. As pointed out in previous studies, other components found in this fibre include an amorphous SiO_xC_y phase and dispersed carbon (BSU's) nanocrystals.[7,22] The deconvolution of the Si 2p photopeak obtained by XPS after etching ~50 nm from the fibre surface accounted for an SiC to SiO_xC_y ratio of 233/110.

On the other hand, the as-received HPZ fibre is completely amorphous, as revealed by the SAED pattern in Fig. 2. The corresponding BF image indicates that the fibre contains some porosity in the 20–50 nm range. A thick (~200 nm) porous layer of different contrast was found on the surface of the HPZ fibres (Fig. 3). Such a layer has been already reported by Chang and Zangvil.[23] AES depth profiles indicated a gradual change in the layer composition from SiO_xC_y to SiN_xC_y with an intermediate $SiO_xC_yN_z$ phase showing up at a depth of 50 nm. XPS analyses were also performed at different sputtering depths from the fibre surface. All Si 2p peaks were found to be

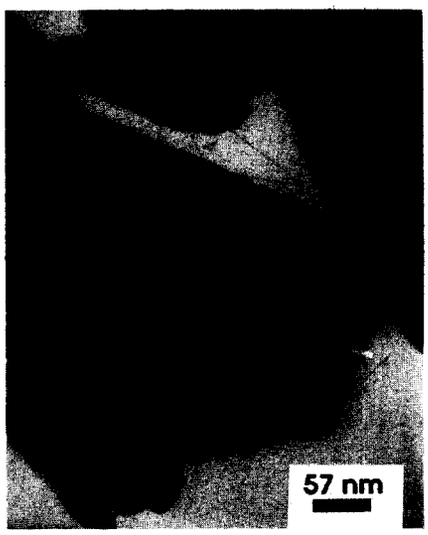

Fig. 3. TEM BF showing the porous surface of the as-received HPZ fibre, as indicated by arrows.

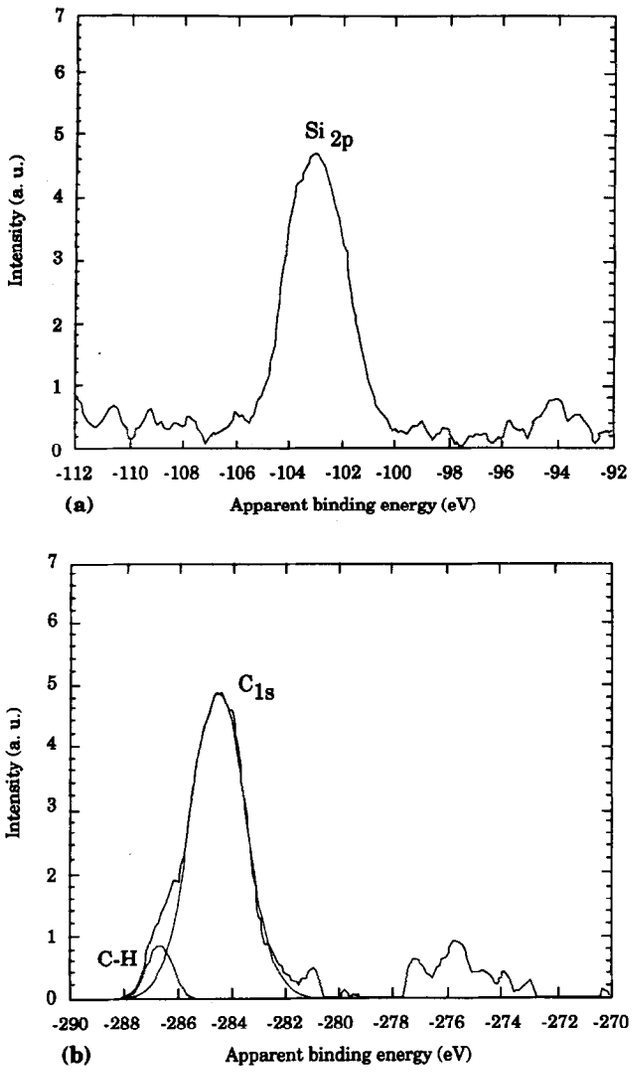

Fig. 4. XPS analysis on as-received HPZ fibres near the surface. (a) Symmetric Si 2p photopeak indicating that Si exists in a single phase. (b) Slightly shifted C 1s photopeak revealing the existence of C–H bonds originating from the polymer precursor.

symmetric, indicating a unique binding nature for Si and suggesting that Si exists in only one phase relatively to the depth. A typical Si 2p photopeak is represented in Fig. 4(a). On the other hand, the *C* 1s peak in Fig. 4(b) presents a second component bearing the feature of C–H or C–CH_3 bonds. This subpeak accounted for ~8 at% of the total carbon.

3.2 Molecular composition of as-received fibres

Attempts to quantitatively determine the fibre molecular composition required some simplifications due to the complexity of these chemical systems. First, based on the experimental observations, the 200 nm thick surface of the HPZ fibre was assumed to contain all the oxygen and its composition was taken as pure SiO_2. Second, the free carbon content in each fibre was estimated from rule-of-mixtures (ROM) calculations (normal ROM compositions can be calculated by assigning all oxygen to silicon as SiO_2; then all nitrogen to silicon as Si_3N_4; then carbon to silicon as SiC; the excess carbon is considered to be in the elemental standard state). An additional relationship, the SiC-to-SiO_xC_y molar ratio obtained by XPS, was also required for the Nicalon fibre. Then, the sets of equations given in Appendix 1 were solved. The solutions shown in Table 1 are expressed as A = mol% SiC, B = mol% SiO_xC_y for Nicalon and SiN_xC_y for HPZ, C = mol% free C, x and y. Finally, a simplification of the ternary phase formulae was performed by establishing an empirical relationship between the coefficients x and y. This led to $y = 1 - (x/2)$ for Nicalon and $y = 1 - (3x/4)$ for HPZ. The resulting formulae, $SiO_xC_{1-(x/2)}$ for Nicalon and $SiN_xC_{1-(3x/4)}$ for HPZ, can be easily verified graphically by means of mixed, $Si(C,O)_4$ or $Si(C,N)_4$, tetrahedal structures, as shown in Figs 5(a) and (b). Let α be the number of Si–O (or Si–N) bonds and $4 - \alpha$ the remaining Si–C bonds per tetrahedron, and assume that unsaturated silicon, Si–Si, O–O, C–O, N–N and multiple bonds are prohibited. The O, N and C contributions per tetrahedron normalized to one Si atom are respectively $\alpha/2$, $\alpha/3$ and $(4 - \alpha)/4$. Finally, let $x = \alpha/2$ leads to the chemical formula $SiO_xC_{1-(x/2)}$ for

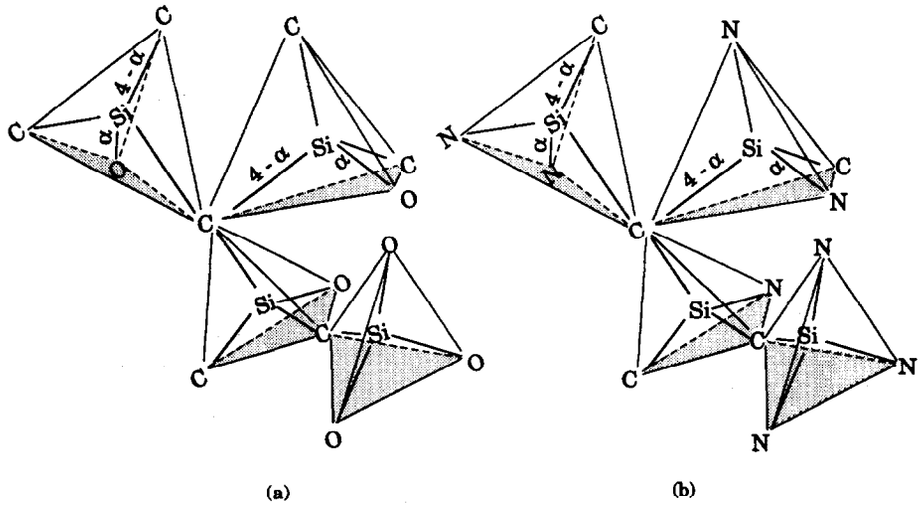

Fig. 5. Three-dimensional structure networks of the ternary glassy phases in the Nicalon and HPZ fibres: (a) SiO_xC_y, (b) SiN_xC_y.

Nicalon. Similarly, let $x = \alpha/3$ leads to $SiN_xC_{1-(3x/4)}$ for HPZ. The α value which represents the average number of oxygen or nitrogen bonded to silicon (the remaining $4 - \alpha$ being carbon bonds) signifies that 2·24 oxygen and 1·76 carbon atoms on one hand, and 3·06 nitrogen and 0·94 carbon atoms on the other hand, are bonded to every silicon atom in the respective ternary phases of the Nicalon and HPZ fibres.

Based on the above proposed formulae for the ternary phases, the fibre molecular compositions can now be varied within some limit values of x. Results are shown in Figs 6(a) and (b) along with the actual fibre compositions (dashed lines). Figure 6(a) shows that SiC vanishes in Nicalon at x = 0·36, resulting in a fibre composed of 72 mol% $SiO_xC_{1-(x/2)}$ and 28 mol% C. The fibre composition at x = 2, on the other hand, corresponds to that calculated from the ROM (mol% SiC = 59, SiO_2 = 13 and C = 28). As shown in Fig. 6(b), the HPZ fibre has the ROM composition at x = 0 and x = 4/3 (mol% SiC = 32·5, Si_3N_4 = 35·5, SiO_2 = 6·8 and free C = 25·2). Moreover, shifting x from these limits reduces both SiC and Si_3N_4 phase contents. The fibre composition at the convergent point where the stoichiometric carbide and nitride phases vanish (x = 1·02) corresponds to the actual composition of the HPZ fibre. Finally, it is shown that the free carbon content in both fibres remains constant within the entire range and thus does not depend on the composition of the other fibre phases.

3.3 Effects of heat treatments on fibre microstructure

3.3.1 Nicalon fibre

The effect of heat treatment on the Nicalon fibre crystallization was revealed by XRD and TEM. An increase of β-SiC crystallinity with ageing temperature and time was represented by a sharpening of the XRD spectrum. At the same time, the TEM analysis revealed an increased average grain size of β-SiC. As shown in Figs 7(a) and (b), the rate of grain growth in both atmospheres was found to increase with temperature and to decrease with exposure time. Figure 7(b) further indicates that a more pronounced crystallinity of β-SiC developed in Nicalon during ageing treatments in argon. An exaggerated grain growth and a well pronounced porosity resulting from exposure for 90 h at 1300°C in argon are shown in Fig. 1. The X-ray diffraction patterns also indicated that cristobalite peaks show up in air. A thick oxide scale on the fibre surface, resulting from exposure for 90 h at 1300°C, is shown in Fig. 8(a). The

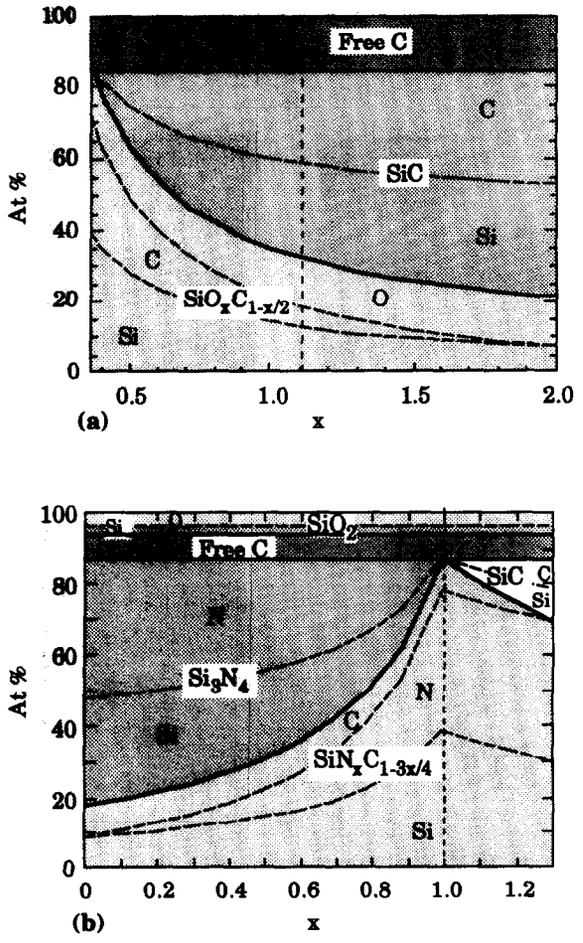

Fig. 6. Predicted variations of the fibre molecular compositions as a function of the parameter x: (a) Nicalon, (b) HPZ.

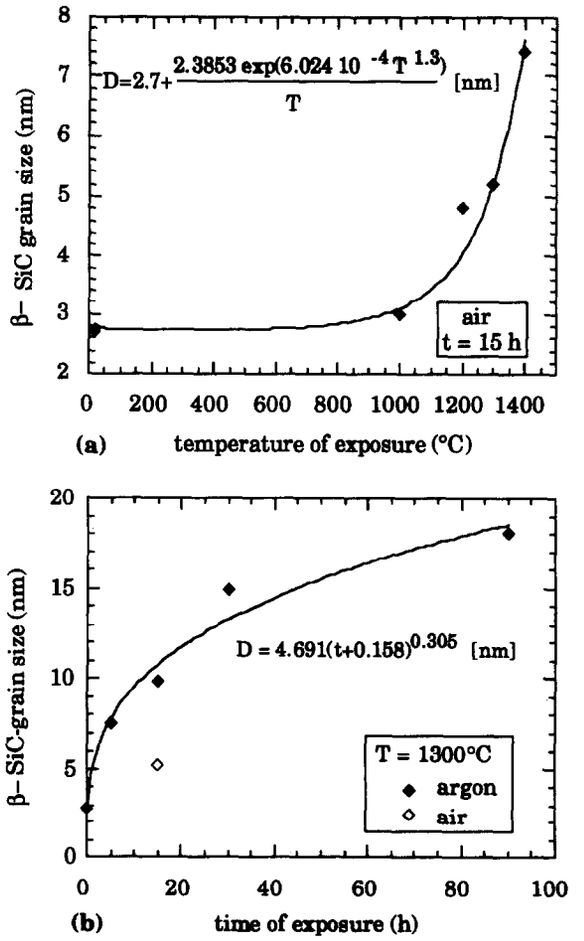

Fig. 7. β-SiC grain growth in the Nicalon fibre as a function of (a) temperature and (b) time of heat treatment in air and argon.

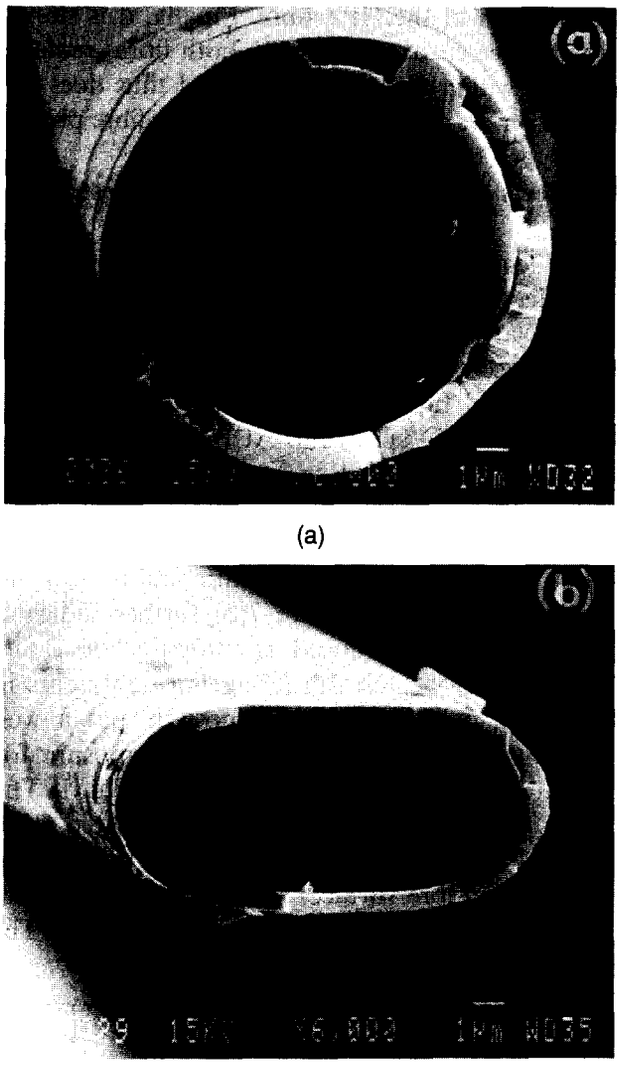

Fig. 8. SEM analysis of the fracture surfaces of fibres heat-treated for 90 h in air at 1300°C. (a) Nicalon, (b) HPZ.

composition of the heat-treated fibres in argon was analysed by means of AES depth profiling. The Nicalon fibre progressively transformed to stoichiometric SiC with increasing heat treatment time. This transformation was complete after 30 h at 1300°C and 15 h at 1400°C.

3.3.2 HPZ fibre

Crystallization of the HPZ fibre did not occur at temperatures below 1300°C in argon. After long heat treatment times at this temperature, microstructural modifications were observed near the fibre surface. A low magnification image of a surface region and the corresponding SAED pattern are shown in Fig. 9. The crystalline phase was identified as being cristobalite. Once cristobalite was transformed to amorphous silica when irradiated by the electron beam, further TEM analyses below the silica crust revealed the existence of two stable crystalline phases, Si_2N_2O and β-SiC, as well as the presence of channels of porosity within the silicon oxynitride phase [Figs 10(a) to (c)]. On

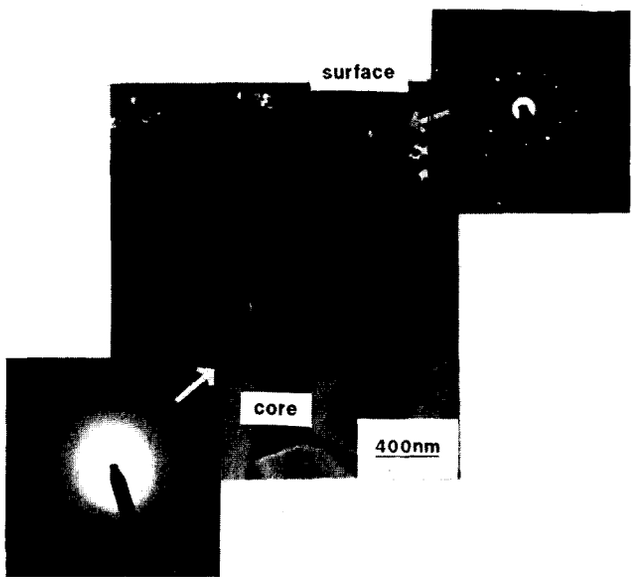

Fig. 9. SiO_2 DF micrograph of an HPZ fibre heat-treated for 90 h at 1300°C in argon, showing the crystallized fibre surface.

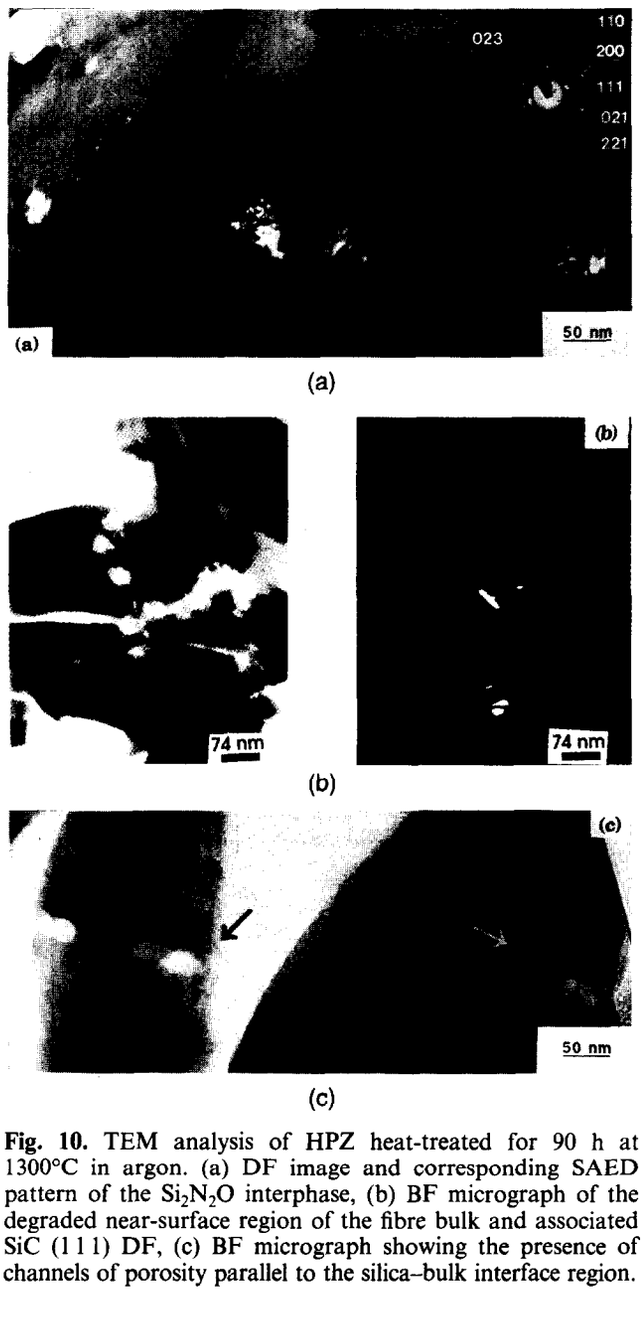

Fig. 10. TEM analysis of HPZ heat-treated for 90 h at 1300°C in argon. (a) DF image and corresponding SAED pattern of the Si_2N_2O interphase, (b) BF micrograph of the degraded near-surface region of the fibre bulk and associated SiC (1 1 1) DF, (c) BF micrograph showing the presence of channels of porosity parallel to the silica–bulk interface region.

Fig. 11. TEM image showing channels of porosity in the oxide reaction layer of an HPZ fibre heat-treated in air for 15 h at 1400°C.

the other hand, the remaining fibre after prolonged heat treatments in argon still bore the characteristics of the as-received fibre, i.e. same bulk composition and same amorphous structure (Fig. 9).

It was very difficult to establish evidence for all these microstructural changes for shorter exposure times in argon, as well as for all heat treatment conditions in air. As shown in Fig. 8(b), cristobalite again developed on the fibre surface in air. The presence of surface-connected channels in this reaction layer was also observed (Fig. 11).

3.4 Effects of heat treatments on fibre strength

Figures 12(a) and (b) show the room temperature strengths and moduli of the two fibres as a function of the exposure time in argon. It is seen from Fig. 12(a) that the heat treatment temperature greatly affected the degree of strength degradation. After heat treatments for 15 h at 1200, 1300 and 1400°C, the average strength of Nicalon was progressively lowered by 46·8, 75·9 and 91%, respectively, compared with that of the as-received fibres. By comparison, the strength of the HPZ fibre showed a decrease of 28·7, 40, and 68·1% at these temperatures. Also, the time of heat treatment was found to have an impact on the rate of strength degradation. During the first 15 h, the strength obviously reduced faster than it did during the rest of the heating period. For Nicalon this phenomenon was in apparent agreement with other changes occurring in the fibre, for example β-SiC grain growth and weight loss. Fig. 12(b) shows that the modulus of Nicalon lost 64% of its initial value after 15 h at 1400°C whereas that of

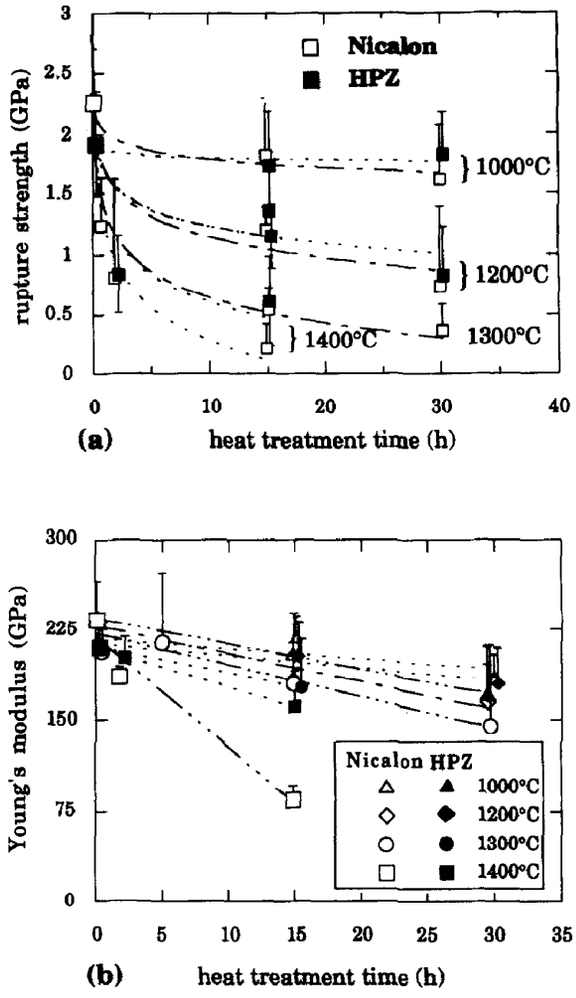

Fig. 12. Effect of time of heat treatment in argon on (a) tensile strength at room temperature and (b) Young's modulus of Nicalon and HPZ fibres. Open symbols represent Nicalon; black symbols represent HPZ. The single-sided bars represent the standard deviations.

HPZ was lowered by only 24% under the same ageing conditions.

3.5 Modelling the decomposition of the Nicalon fibre

To a large extent, heat treatments in inert atmospheres can be regarded as a continuation of the fibre pyrolysis. Many of the events taking place during heat treatments of Nicalon also occur during the last stage of pyrolysis. Among them are the crystallization of β-SiC, weight loss of the fibre, and CO and SiO evolution.[9] However, unlike pyrolysis — which is controlled to optimize the fibre properties — prolonged heat treatments often result in fibre degradation.

The overall decomposition of the Nicalon fibre can be expressed as

$$Si_{0.72}O_{0.26}C_{0.87} = (n_{SiC} + \Delta n_{SiC})\ SiC + (n_C + \Delta n_C)\ C + \Delta n_{CO}\ CO + \Delta n_{SiO}\ SiO \quad (1)$$

where $Si_{0.72}O_{0.26}C_{0.87}$ is the fibre molar formula and n_{SiC} and n_C are the initial mole ratios of SiC and C (see Table 1). Δn_{SiC}, Δn_C, Δn_{CO} and Δn_{SiO} are the variations of the mole ratios of the products.

The simplest approach used to model the decomposition is to consider the stepped progression of reaction (1) into the fibre (i.e. layer by layer), and to assume that one layer is fully decomposed when all the carbon has been consumed, i.e. $n_C + \Delta n_C = 0$. The results are shown in Figs 13(a) and (b) as a function of the molar percentage of decomposed fibre, along with the related changes in weight loss, density and porosity, which were obtained from

$$\Delta W/W_0 = \frac{\Delta W_{CO} + \Delta W_{SiO}}{M_0} = \frac{28\,\Delta n_{CO} + 44\,\Delta n_{SiO}}{M_0} \quad (2)$$

$$\rho_f = \rho_0(1-\Delta W/W_0) \quad (3)$$

$$P = 1 - \frac{\rho_f}{\Sigma\, V_i\rho_i} = 1 - \frac{\rho_f}{V_{SiC}\,\rho_{SiC} + V_C\,\rho_C + V_g\,\rho_g} \quad (4)$$

where $\Delta W_{CO} + \Delta W_{SiO}$ is the total weight of gas released, M_0 is the molar weight of the Nicalon fibre (M_0 = 34·8 g mol^{-1}), ρ_0 is the initial fibre density (ρ_0 = 2·55 g cm^{-3}), V_i is the volume fraction of the ith component ($V_i = m_i/\rho_i = n_iM_i/\rho_i$), ρ_{SiC} = 3·20 g cm^{-3}, ρ_C = 1·80 g cm^{-3}, and ρ_g is the density of the silicon oxycarbide glass which has been estimated from $\rho_0 = \Sigma V_{i\rho i}$, assuming an initial porosity of 2% in accordance with Ref. 7. The value obtained for ρ_g, i.e. 2·18 g cm^{-3}, was found to be slightly smaller than that of silica, for which ρ_{SiO_2} = 2·20 g cm^{-3}.

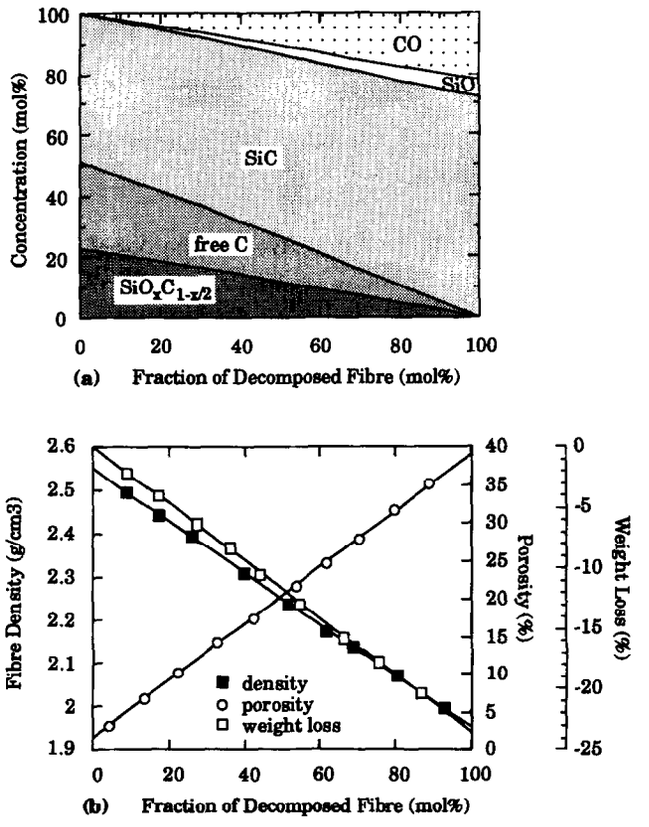

Fig. 13. Predicted variations of (a) the mole fractions of the chemical phases and (b) the porosity, density and weight loss as a function of the fraction of decomposed Nicalon fibre.

Finally, the calculated weight loss data were fitted with the experimental ones in order to plot the decomposition predictions on a time scale. The results are shown in Figs 14 and 15 for different test temperatures. In Fig. 14, the rate of decomposition is clearly expressed by the evolution of the gas phases (SiO + CO). This evolution remains limited at 1200°C even after long exposure times (~100 h). The decomposition is much faster at higher temperature and has practically ended after ~12 h at 1300°C and only ~1 h at 1400°C as it reaches a plateau which corresponds to the total consumption of carbon and silicon oxycarbide. The predicted variations of the density

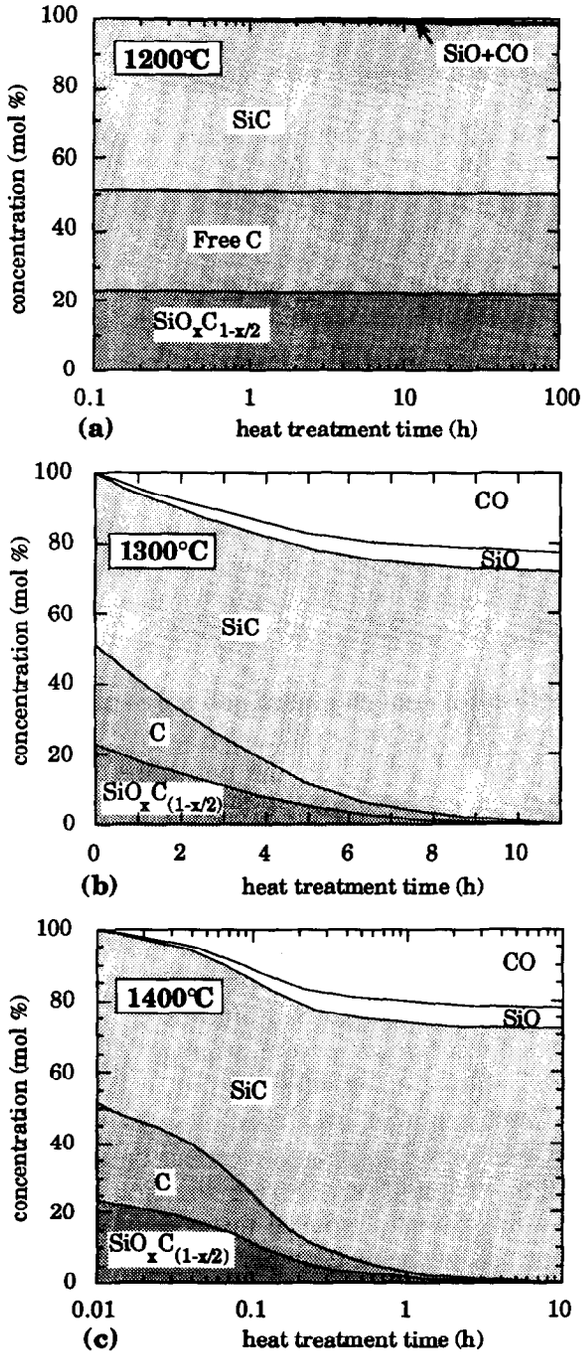

Fig. 14. Predicted variations of the molecular composition of Nicalon as a function of the exposure time in argon at (a) 1200°C, (b) 1300°C and (c) 1400°C.

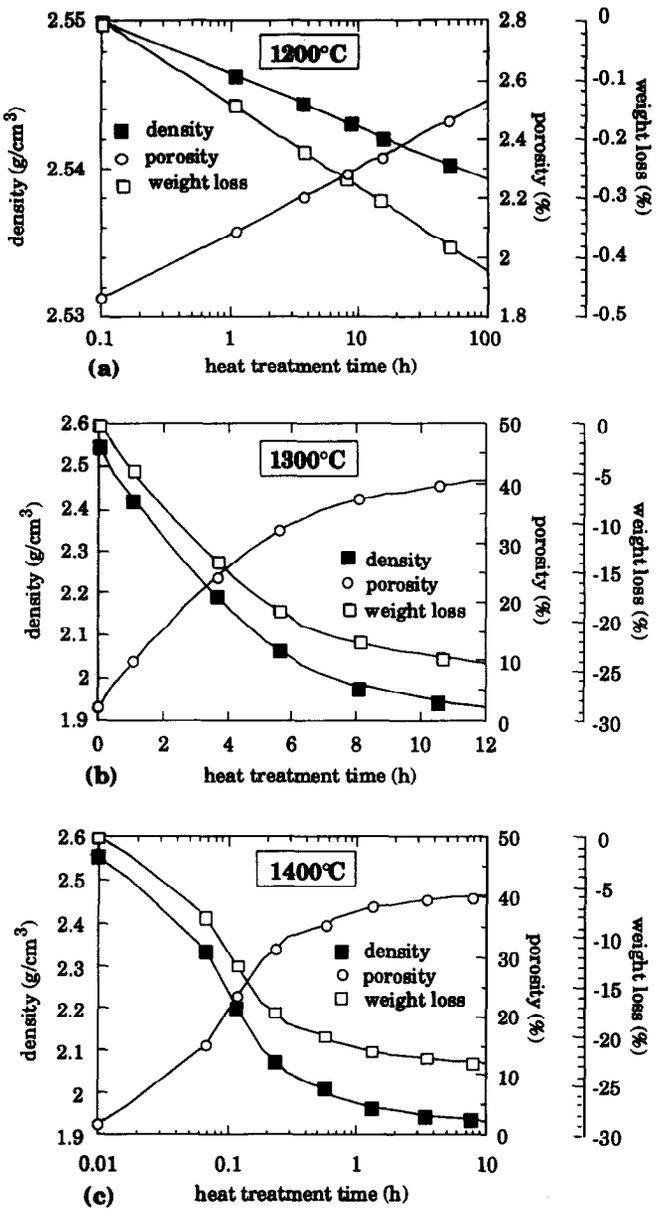

Fig. 15. Evolution of the density and porosity predicted from the experimental weight loss curve for the Nicalon fibre as a function of time of exposure in argon: (a) 1200°C, (b) 1300°C and (c) 1400°C.

and porosity along with the experimental weight loss curves are shown in Fig. 15. At the points where the experimental weight loss curves level off, the final density has dropped to ~1·9 g cm^{-3} whereas the porosity has increased to ~40%.

4 Discussion

4.1 As-received fibres

The determination of the free carbon content from rule-of-mixtures calculations is questionable. It was, however, shown in Fig. 6 that a variation of composition of the other fibre phases does not effect its initial content. Schreck *et al.*[22] attempted to determine from XPS analyses the molecular composition of the as-received Nicalon fibre. The ranges of x and y, for the silicon oxycarbide phase, were found to be $x = 1{\cdot}20 \pm 0{\cdot}11$ and $y = 0{\cdot}39 \pm 0{\cdot}06$. The empirical values obtained in the present study, $x = 1{\cdot}12$ and $y = 0{\cdot}44$, lie perfectly in these ranges. These data further correlate with the proposed relationships, $y = 1 - (x/2)$ for Nicalon and $y = 1 - (3x/4)$ for HPZ, established graphically (Fig. 5).

The porous structure and the heterogeneous oxygen-rich surface of the HPZ fibre detected by TEM and AES have already been reported.[23] Depending on processing conditions, the SiO_2-rich surface layer can be 0·1 to 0·7 μm thick. Band II in the C 1s XPS spectrum [Fig. 4(b)] suggests that carbon species carrying hydrogen or methyl groups may exist in HPZ due to incomplete decomposition of the organic precursor. It was reported that the residual hydrogen in this fibre could be as high as 0·1 wt% (~2 at%).[14] The corresponding H/C atomic ratio, i.e. 8%, has been confirmed here by XPS.

4.2 Thermal degradation of fibres

4.2.1 Nicalon fibre

Based on the microstructural observations, it is likely that the mechanical properties of Nicalon are controlled predominantly by the gradual decomposition of SiO_xC_y from the surface at elevated temperatures. If the gas diffusion is faster near the fibre surface than near the centre, the same will be true for the grain growth. This supposition was confirmed by the experimental observations which indicated a gradual grain growth in the heat-treated fibres (Fig. 1). Thus, the decomposition and related grain growth will proceed further in the fibre with time of heat treatment. The assumption used in quantification of the decomposition, that carbon is fully reacting in reaction (1), leads to a good agreement between the predicted and the experimental total weight losses (23·5 wt% vs. 24 wt%). It furthermore implies that the maximum CO is generated and results in a CO/SiO molar ratio of ~4 [Fig. 13 (a)]. This fact confirms previous statements that the major gas released from the Nicalon fibre is CO.[24]

The SiC crystallization may be reduced in air due to the formation of an oxidation layer on the fibre surface. This compact silica layer may retain the gas and consequently slow down the decomposition reaction.

4.2.2 HPZ fibre

The bulk of the HPZ fibre exhibited structural stability for all heat treatment conditions. On the

other hand, the crystallization of the surface into cristobalite, silicon oxycarbide and to a lesser extent silicon carbide was observed after prolonged exposures in argon (Figs 9 and 10). The presence of Si_2N_2O has also been noticed in HPZ/LAS matrix composites.[18,19] This phase was believed to arise from some fibre–matrix interfacial reactions. The slow formation of Si_2N_2O and SiC may be explained by the occurrence of solid-state reactions at the silica–bulk interface in the fibre, such as:

$$\frac{4}{x}\,SiN_xC_{1-(3x/4)} + SiO_2 \rightarrow 2\,Si_2N_2O + \left(\frac{4}{x} - 3\right) SiC \quad (5)$$

The stability of the silica–bulk interface is likely to persist for a long time during heat treatment because of the slow kinetics of reaction (5) which leads to the crystalline equilibrium composition.

The formation of SiC may also arise from the fibre bulk decomposition according to:

$$4\,SiN_xC_{1-(3x/4)} + 3x\,C \rightarrow 2x\,N_2(g) + 4\,SiC \quad (6)$$

In addition, reaction (6) yields nitrogen gas. Previous thermodynamic calculations indicated that the nitrogen partial pressure could be as high as 10^{-1} bar at 1300°C above Si–C–N–O fibres with an excess of carbon.[24] However, the oxide layer on the HPZ fibre may provide a good diffusion barrier for the gas. Since the β-SiC crystals were only observed after long treatments (Fig. 10), it is likely that an accumulation of N_2 prevented the formation of SiC until the gas pressure became sufficiently low for reaction (6) to proceed to the right. Where it is not related to the spinning defects, the porosity found in the near-surface region may be related to gas evolution (Figs 10 and 11).

In air, the reactions (7) and (8) are believed to occur simultaneously:

$$4\,SiN_xC_{1-(3x/4)} + \left(6 - \frac{3x}{2}\right) O_2 \rightarrow 4\,SiO_2 + (4 - 3x)CO + 2x\,N_2 \quad (7)$$

$$C + O_2 \rightarrow CO_2 \quad (8)$$

As far as the oxidation resistance is concerned, oxygen diffusion through Si_2N_2O is more difficult than through silica.[25] Thus, Si_2N_2O will provide a good protection barrier against oxidation. The thinner reaction layer on HPZ compared with Nicalon under the same heat treatment conditions supports this assumption (Fig. 8).

4.3 Strength degradation

The tensile properties of Nicalon degraded more severely than those of HPZ during heat treatments in argon. This degradation is attributed to the gradual decomposition of the SiO_xC_y phase from the surface, which causes grain growth and forms intergranular porosity. The rate of strength degradation increased with temperature and decreased with time (Fig. 12), similarly to the rate of grain growth (Fig. 7) and porosity (Fig. 15). The low modulus of Nicalon heat-treated under the most severe conditions may result from the quasi-absence of cohesion between SiC crystals due to replacement of the intergranular residual carbon and silicon oxycarbide phases by porosity.

On the other hand, the amount of compositional change was immeasurably small in the case of HPZ fibres after ageing in argon, and it is clear from the microstructural analyses that surface damage was responsible for most of the strength loss. This damage may arise during cooling from the thermal expansion mismatch between the crystallized species of the surface, i.e. cristobalite and silicon oxynitride, on one hand, and the glassy phase of the fibre bulk, on the other hand. Additionally, the porosity related to the gas evolution resulting from the bulk decomposition certainly affected the fibre mechanical properties. It is suggested that the time-dependent strength of the HPZ fibre resulted from the slow kinetics of solid–solid reactions, such as reactions (5) and (6).

5 Summary and Conclusions

The most significant results of this study can be summarized as follows.

(1) Based on the elemental and structural analyses, the molecular compositions of the Nicalon and HPZ fibres have been determined. It is proposed that the Nicalon fibre consists of three phases which are SiC, C and a $SiO_{1.12}C_{0.44}$ phase, the corresponding molar percentages of which are 49, 28 and 23. Assuming again a three-phase material for the HPZ fibre, its composition has been taken as SiO_2 = 4 mol%, $SiN_{1.02}C_{0.23}$ = 81 mol% and C = 15 mol%. It is suggested that the amorphous ternary phases can be represented by the formulae $SiO_xC_{1-(x/2)}$ and $SiN_xC_{1-(3x/4)}$ for Nicalon and HPZ, respectively. The experimental observations revealed that the HPZ fibre is amorphous, inhomogeneous in surface composition, and that it contains processing defects, such as a 200 nm thick silica-rich layer on the surface and small globular pores at the nanometre scale in the bulk.

(2) Heat treatments were performed on fibres in air and argon from 0·5 to 90 h between 1000°C and 1400°C. In Nicalon, the grain

growth was much faster in argon than in air, and it was much more sensitive to an increase in temperature than to a prolonged treatment. The gradual evolution of porosity in this fibre also decreased with time of heat treatment. Heat treatments of HPZ in argon resulted in the crystallization of the near-surface region into α-cristobalite, Si_2N_2O and β-SiC, and in the development of microporosity. It was suggested that the Si_2N_2O and SiC formations in HPZ are controlled by the slow kinetics of solid-state reactions involving the oxygen-rich scale, the silicon carbonitride and the free carbon of the bulk. On the other hand, the HPZ fibre core showed structural stability up to 1400°C.

(3) The strength degradation was for Nicalon in apparent agreement with other changes occurring in the fibre, for example β-SiC grain growth and weight loss. While the internal porosity may have contributed to the lower room temperature strength of the HPZ fibre compared with Nicalon, its strength degradation in argon was only related to surface degradation.

Acknowledgements

The authors would like to thank the Gas Research Institute for financially sponsoring this project through the Center for Advanced Materials at Penn State University, and the Société Européenne de Propulsion for a grant given to R. B. They acknowledge the assistance of Dr H. Du of the Stevens Institute of Technology for conducting the AES and XPS analyses.

References

1. Yajima, S., Hayashi, J. & Omori, M., Continuous silicon carbide fiber of high tensile strength. *Chem. Lett.*, **9** (1975) 931–4.
2. Villeneuve, J. F., Mocaer, D., Pailler, R., Naslain, R. & Olry, P., Tensile testing at high temperatures of ex-PCS Si–C–O and ex-PCSZ Si–C–N single filaments. *J. Mater. Sci.*, **28** (1993) 1227–36.
3. Sawyer, L. C., Microstructure of ceramic fibers. In *Fibre Reinforced Ceramic Composites*, ed. K. S. Mazdiyasni. Noyes Publications, Mill Road, NJ, 1990, pp. 141–81.
4. Pysher, D. J., Goretta, K. C., Hodder Jr, R. S. & Tressler, R. E., Strengths of ceramic fibers at elevated temperatures. *J. Am. Ceram Soc.*, **72** (1989) 284–8.
5. Kim, H. E. & Moorhead, A. J., Strength of Nicalon carbide fibers exposed to high-temperature gaseous environments. *J. Am. Ceram. Soc.*, **74** (1991) 666–9.
6. Shimoo, T., Chen, H. & Okamura, K., Pyrolysis of Si–C–O fibres (Nicalon) at temperature from 1473 K to 1673 K. *J. Ceram. Soc. Japan.*, **100** (1992) 48–53.
7. Le Coustumer, P., Monthioux, M. & Oberlin, A., Understanding Nicalon fibre. *J. Eur. Ceram. Soc.*, **11** (1993) 95–103.
8. Chaim, R., Heuer, A. H. & Chen, R. T., Microstructural and microchemical characterization of silicon carbide and silicon carbonitride ceramic fibers produced from polymer precursors. *J. Am. Ceram Soc.*, **71** (1988) 960–9.
9. Langley, N. R., LeGrow, G. E. & Lipowitz, J., Properties of ceramic fibers from organosilicon polymers. In *Fiber Reinforced Ceramic Composites*, ed. K. S. Mazdiyasni. Noyes Publications, Mill Road, NJ, 1990, pp. 63–92.
10. Jia, N., Bodet, R. & Tressler, R. E., Effects of microstructural instability on the creep behavior of Si–C–O (Nicalon) fibers in argon. *J. Am. Ceram. Soc.*, **76** (1993) 3051–60.
11. Bodet, R., Jia, N. & Tressler, R. E., Thermomechanical stability of Nicalon fibres in a carbon monoxide environment. *J. Eur. Ceram. Soc.*, **15** (1995) 997–1006.
12. Bodet, R., Lamon, J. & Tressler, R. E., Effects of chemical environments on the creep behavior of Si–C–O fibres. In *Proceedings of the 1st International Conference on High Temperature Ceramic Matrix Composites*, ed. R. Naslain, J. Lamon & D. Doumeingts. Woodhead Publishing, Cambridge, 1993, pp. 75–83.
13. Bodet, R., Lamon, J., Jia, N. & Tressler, R. E., Microstructural stability and creep behavior of Si–C–O (Nicalon) fibers in carbon monoxide and argon environments. *J. Am. Ceram. Soc.*, in press.
14. Lipowitz, J., Freeman, H. A., Chen, R. T. & Prack, E. R., Composition and structure of ceramic fibers prepared from polymer precursors, *Adv. Ceram. Mater.*, **2** (1987) 121–8.
15. Langley, N. R. & Li, C. T., Effects of interfacial diffusion barriers on thermal stability of ceramic fibers. In *Ceramic Microstructure '86, Role of Interfaces*, ed. J. A. Pask & A. G. Evans. Plenum Press, New York, 1987, pp. 401–7.
16. Lin, W. & Yang, J. M., Thermal stability of ceramic fibre in a CVI-processed SiC matrix composite. *J. Mater. Sci.*, **26** (1991) 4116-22.
17. Lane, J. E. & Pebler, A. R., Failure characteristics of low dielectric constant ceramic composites reinforced with BN-coated fibers. *Ceram. Eng. Sci. Proc.*, **10** (1989) 1213–22.
18. Brennan, J. J., Interfacial characteristics of glass-ceramic matrix/SiC fibre composites. *J. de Physique*, **49** (1988) 791–809.
19. Brennan, J. J., Glass and glass-ceramic matrix composites. In *Fiber Reinforced Ceramic Composites*, ed. K. S. Mazdiyasni. Noyes Publications, Mill Road, NJ, 1990, pp. 222–59.
20. Lewis, M. H. & Murthy, V. S. R., Microstructural characterization of interfaces in fiber-reinforced ceramics. *Compos. Sci. Technol.*, **42** (1991) 221–49.
21. Li, C. T. & Langley, N. R., Improvement in fiber testing of high-modulus single filament materials. *J. Am. Ceram. Soc.*, **68** (1985) C202–4.
22. Schreck, P., Vix-Guterl, C., Ehrburger, P. & Lahaye, J., Reactivity and molecular structure of silicon carbide fibres derived from polycarbosilanes. Part II: XPS analysis. *J. Mater. Sci.*, **27** (1992) 4243–6.
23. Chang, Y. W. & Zangvil, A., Characterization of Si–C–N–O fibers by analytical STEM and scanning Auger techniques. In *Ceramic Transactions, Silicon Carbide '87*, ed. J. D. Cawley & C. E. Semler. The American Ceramic Society, Westerville, OH, 1989, pp. 435–43.
24. Luthra, K. L., Thermomechanical analysis of the stability of continuous 'SiC' fibers. *J. Am. Ceram. Soc.*, **9** (1986) C231–3.
25. Tressler, R. E., Spear, K. E., Zheng, Z. & Du, H., Fundamental studies of the oxidation of silicon carbide crystals and CVD silicon nitride. In *High Temperature Corrosion of Technical Ceramics*, ed. R. J. Fordham. Elsevier Applied Science, London, 1990, pp. 69-89.

APPENDIX 1

The fibre molecular compositions given in Table 1 were obtained by solving the following sets of equations.

For the Nicalon fibre:

$$\text{Si} = \frac{39}{100} = \frac{A + B}{2A + B(y + 1 + x) + C} \quad \text{(A1)}$$

$$C_{\text{free}} = \frac{15}{100} = \frac{C}{2A + B(y + 1 + x) + C} \quad \text{(A2)}$$

$$\text{O} = \frac{14}{100} = \frac{xB}{2A + B(y + 1 + x) + C} \quad \text{(A3)}$$

$$C_{\text{bonded}} = \frac{32}{100} = \frac{A + yB}{2A + B(y + 1 + x) + C} \quad \text{(A4)}$$

$$\frac{A}{B} = \frac{233}{100} \quad \text{(from XPS analysis)} \quad \text{(A5)}$$

$$A + B + C + 1 \quad \text{(A6)}$$

with SiC = A, SiO_xC_y = B, free carbon = C.

For the HPZ fibre:

$$\text{Si} = \frac{40}{100} = \frac{A + B}{2A + B(y + 1 + x) + C} \quad \text{(A7)}$$

$$C_{\text{free}} = \frac{7}{100} = \frac{C}{2A + B(y + 1 + x) + C} \quad \text{(A8)}$$

$$\text{O} = \frac{4}{100} = \frac{2A}{2A + B(y + 1 + x) + C} \quad \text{(A9)}$$

$$\text{N} = \frac{40}{100} = \frac{xB}{2A + B(y + 1 + x) + C} \quad \text{(A10)}$$

$$C_{\text{bonded}} = \frac{9}{100} = \frac{yB}{2A + B(y + 1 + x) + C} \quad \text{(A11)}$$

$$A + B + C + 1 \quad \text{(A12)}$$

with SiO_2 = A, SiN_xC_y = B, free carbon = C.